Journal of Solid State Chemistry 182 (2009) 3374–3382

Contents lists available at ScienceDirect

Journal of Solid State Chemistry

journal homepage: www.elsevier.com/locate/jssc

Order–disorder transition and valence state of ytterbium in $YbAu_xGa_{2-x}$ ($0.26 \le x \le 1.31$)

R. Gumeniuk [a,*], E. Bischoff [b], U. Burkhardt [a], Yu. Prots [a], W. Schnelle [a], L. Vasylechko [c], M. Schmidt [a], Yu. Kuzma [d,†], Yu. Grin [a]

[a] Max-Planck-Institut für Chemische Physik fester Stoffe, Nöthnitzer Str. 40, 01187 Dresden, Germany
[b] Max-Planck-Institut für Metallforschung, Heisenbergstr. 3, 70569 Stuttgart, Germany
[c] Lviv Polytechnic National University, Bandera Str. 12, 79013 Lviv, Ukraine
[d] Department of Analytical Chemistry, Ivan Franko National University of Lviv, Kyryla & Mefodija Str. 6, 79005 Lviv, Ukraine

ARTICLE INFO

Article history:
Received 17 June 2009
Received in revised form
10 September 2009
Accepted 13 September 2009
Available online 19 September 2009

Keywords:
Gallide
Ytterbium
Crystal structure
Phase transition
Magnetism
XAS spectra
Order–disorder

ABSTRACT

The intermetallic compounds $YbAu_xGa_{2-x}$ ($0.26 \le x \le 1.31$) were synthesized by melting of elemental components and subsequent annealing. The crystal structure of $YbAu_{1.04}Ga_{0.96}$ was investigated using single-crystal X-ray diffraction data: structure type TiNiSi, space group *Pnma*, a=7.1167(3) Å, b=4.5019(3) Å, c=7.7083(3) Å, R_F=0.028 for 27 variables and 441 reflections. At 600 °C this compound is described as partially substituted TiNiSi type and shows a homogeneity range around the equiatomic composition $YbAu_xGa_{2-x}$ ($0.94 \le x \le 1.19$). For the gallium- ($0.26 \le x \le 0.83$) and gold-rich ($1.21 \le x \le 1.31$) regions, the KHg_2 type of crystal structure (space group *Imma*) with mixed Au/Ga occupation is found. A temperature-driven phase transition for the composition YbAuGa from ordered TiNiSi to disordered KHg_2 structure type is observed at 629 °C. Yb L_{III} X-ray absorption spectra indicate an intermediate valence of +2.5 for Yb atoms in YbAuGa. For samples deviating from this composition a further reduced valence of Yb is observed. Magnetic susceptibility studies show a non-magnetic $4f^{14}$ ground state of Yb atoms with thermal fluctuations towards the $4f^{13}$ state.

© 2009 Elsevier Inc. All rights reserved.

1. Introduction

Two phases in the ternary Yb–Au–Ga system have been reported recently to crystallize with orthorhombic KHg_2 structure (space group *Imma*): YbAuGa [1,2] and $YbAu_{0.5}Ga_{1.5}$ [3]. Taking into account the analogy with the large family of equiatomic intermetallic compounds [4] one can assume that the Yb atoms occupy position 4*e* and Au and Ga atoms are statistically distributed in the 8*h* site, which correspond to the K and Hg positions, respectively. The comparision of the unit cell volume of both phases (calculated from unit cell parameters given in [2,3]) unexpectedly showed that the unit cell volume of the Au-rich compound (YbAuGa, V=246.3 Å^3) is slightly smaller than the value obtained for the Au-poor phase ($YbAu_{0.5}Ga_{1.5}$, V=248.1 Å^3), which is in contradiction with the atomic radii of 1.44 Å and 1.22 Å [5] for Au and Ga atoms, respectively.

In the beginning of the present investigation we hoped to find an ordered variant for the equiatomic YbAuGa, as is the case for numerous ternary equiatomic compounds [4]. A further task was to check if the observed anomaly of the unit cell volume is connected to a change of the valence state of ytterbium in the $YbAu_xGa_{2-x}$ phases. Some preliminary results of this work were presented in a conference contribution [6].

2. Experimental

2.1. Sample preparation and lattice parameters

A series of samples with nominal compositions $YbAu_xGa_{2-x}$ ($0.21 \le x \le 1.35$) was prepared from ingots of ytterbium (Dr. Lamprecht, 99.9%), gold foil (Chempur, 99.9%) and gallium granules (Chempur, 99.999%) by using two synthesis routes. In the first procedure, starting components were melted in glassy carbon crucibles under purified argon atmosphere by using a high-frequency furnace. The total mass of each sample was about 1 g and mass losses after the melting procedure were not larger than 0.4%. The obtained buttons were wrapped in molybdenum foil and enclosed in evacuated silica tubes. The thermal treatment was carried out at 600 °C for 720 h with subsequent quenching in cold water. Alternatively, some alloys were prepared by reaction of elemental components in sealed tantalum tubes under argon atmosphere. To prevent oxidation of the tantalum tubes during

* Corresponding author. Fax: +49 351 46464002.
E-mail address: gumeniuk@cpfs.mpg.de (R. Gumeniuk).
† Deceased.

0022-4596/$ - see front matter © 2009 Elsevier Inc. All rights reserved.
doi:10.1016/j.jssc.2009.09.015

the heat treatment they were sealed into evacuated silica ampoules. The starting mixtures were heated up to 1100 °C within 20 h and held at this temperature for 1 h. Then the samples were cooled down to 600 °C within 5 h and subsequently annealed at this temperature for 720 h. Several samples with the equiatomic compositions were annealed at temperatures of 900 °C and 1100 °C for 120 h with the purpose to stabilize a high-temperature modification. The Ta tubes with the samples of this series were quenched in cold water after crushing of the quartz ampoules. Due to the sensitivity of elemental ytterbium to oxygen and moisture all manipulations were carried out in an argon-filled glove box (MBraun, $p(O_2/H_2O) \leq 1$ ppm). The light grey coloured samples $YbAu_xGa_{2-x}$ after preparation are stable in air for a long period of time.

All samples were characterized by X-ray powder diffraction performed on a HUBER imaging plate Guinier camera ($CuK\alpha_1$ radiation, 2θ interval of $6-100°$, exposure time 6×15 min, LaB_6 as internal standard (a=4.15692 Å)). The lattice parameters were refined by least-squares methods using the program package WinCSD [7].

High-temperature diffraction experiments using synchrotron radiation were performed on the sample with equiatomic composition. A set of powder patterns was recorded at beamline B2, HASYLAB, DESY in Debye-Scherrer mode in the temperature interval of $150-790$ °C and 2θ range of $7.5-40.0°$ with a step width of 0.004° by use of the on-site readable image plate detector OBI [8]. The wavelength of 0.49953 Å was determined from five reflections of a Si standard (NIST 640*c*, a=5.431195(9)Å).

2.2. Preparation of the single crystals

The samples obtained with the above-described methods were microcrystalline and did not contain specimens suitable for crystal structure investigation. Single crystals of $YbAu_{1.04}Ga_{0.96}$ were obtained by annealing of the melted buttons at 600 °C for 4 h in a water-cooled silica tube using a high-frequency equipment as described in Ref. [9]. All reflections on the Guinier powder diagram obtained directly after this procedure can be easily indexed on the basis of primitive unit cell corresponding to the structure type TiNiSi. One can distinguish two groups of the reflections: sharp reflections with $h+k+l=2n$ typical for the body-centred KHg_2-like subcell and relatively strong but fuzzy primitive superstructure reflections ($h+k+l \neq 2n$). The latter can be attributed to a partial order of gold and gallium atoms. To achieve full ordering in the distribution of Au and Ga this specimen was subsequently annealed at 600 °C for 720 h. After this treatment all reflections on the X-ray powder diagram of the annealed sample were sharp with comparable full-widths at half maximum (FWHM).

2.3. Crystal structure refinement

Irregular-shaped single crystals of $YbAu_{1.04}Ga_{0.96}$ were mechanically extracted from the annealed sample and their quality was checked by Laue photographs. Data collection was performed on a STOE IPDS diffraction system ($AgK\alpha$ radiation) by oscillation of the selected specimen around the φ axis. The intensities of the reflections were corrected for absorption using an optimized description of the crystal shape [10].

On basis of the obtained lattice parameters, analysis of systematic absences of reflections in the collected data set (possible space groups *Pnma* and $Pna2_1$) as well as the character of X-ray powder diagrams we concluded that the compound $YbAu_{1.04}Ga_{0.96}$ is isostructural with TiNiSi [11]. Atomic positions of γ -YbPtGa [12] were used as starting values for a crystal structure refinement. All relevant information concerning data collection and handling are listed in Table 1. A small amount of gold partially replaces gallium in its position. The resulting atomic coordinates and displacement parameters are presented in Table 2. Selected interatomic distances calculated by using lattice parameters obtained from powder X-ray diffraction data are listed in Table 3.

Table 1
Crystallographic data for $YbAu_{1.04}Ga_{0.96}$.

Composition	$YbAu_{1.040(3)}Ga_{0.960(3)}$
Structure type	TiNiSi
Space group	*Pnma* (no. 62)
Unit cell parameters[a]	
a (Å)	7.1167(3)
b (Å)	4.5019(3)
c (Å)	7.7083(3)
V (Å^3)	246.96(4)
Formula units/cell, Z	4
Calculated density, (g/cm^3)	11.80
Diffraction system	STOE IPDS
Radiation, λ (Å)	Ag$K\alpha$, 0.56087
$2\theta_{max}$ and $(\sin\theta/\lambda)_{max}$	51.43°, 0.774
Absorption correction	numerical
Measured range in h, k, l	±10, ±6, ±11
T(max)/T(min)	2.06
N(hkl) measured	3445
N(hkl) unique	526
R(int)/$R(\sigma)$	0.058/0.025
N(hkl) observed	441
Observation criteria	$F(hkl) > 4.00\sigma(F)$
Extinction parameter	0.0089(6)
Refined parameters	27
$R(F)$	0.028

[a] X-ray powder diffraction data.

2.4. Microstructure investigations

Specimens for a metallographic study were prepared by successive grinding, polishing and finishing (1/4 μm diamond abrasives) of pieces of the annealed samples. Diamond suspension and lubricants appropriate for moisture-sensitive materials were applied during the microstructure preparation. Hot mounting was used to embed the samples in conductive resin. The microstructures were characterized by light-optical microscopy (Zeiss Axioplan 2) and scanning electron microscopy (SEM FEI Philips XL30). The standardless energy-dispersive X-ray spectroscopical analysis (EDXS) was performed with the Si(Li) detector of the EDXS system (Ametek, Genesis Vers.4.6) attached to the SEM. The spectra were recorded at an acceleration voltage of 25 keV with the LaB_6 cathode. The chemical composition is calculated from the ZAF corrected intensities of the Yb*L*, Au*L* and Ga*K* lines. The relative accuracy of the intensity measurements is not better than 1.5% due to the statistical error. This gives a systematic inaccuracy of 0.5 at. % for the content of each element.

Electron backscattering diffraction analysis (EBSD) in combination with automated crystal orientation mapping (ACOM) was performed with a LEO 438 VP scanning electron microscope equipped with a TSL/EDAX OIM^{TM} System (Version 4.5). A sufficient surface quality for pattern formation was realized by additional ion-beam etching. The SEM was operated at 20 kV with 4 nA beam current. EBSD pattern have been acquired and indexed in 50 ms and the computer program performed the discrimination of the different phases by calculating the best fit of calculated and measured bands. The accumulated orientation data can be displayed in a map showing the image quality (IQ) of EBSD patterns, as an orientation or inverse pole figure (IPF) map, or as a

Table 2
Atomic coordinates and displacement parameters (in Å^2) in $YbAu_{1.04}Ga_{0.96}$.[a]

Atom	Site	x	y	z	B_{11}	B_{22}	B_{33}	B_{13}	B_{iso}
Yb	4c	0.0052(1)	1/4	0.7047(1)	0.47(3)	0.70(3)	0.73(3)	−0.01(2)	0.64(2)
Au	4c	0.2888(1)	1/4	0.4092(1)	0.84(3)	0.56(2)	0.65(2)	0.07(2)	0.68(1)
T(3.86(1)Ga+0.14(1)Au)	4c	0.1886(3)	1/4	0.0809(3)	1.15(7)	0.62(6)	0.51(6)	0.00(5)	0.76(4)

[a] $B_{12}=B_{23}=0$ for all atoms.

Table 3
Selected interatomic distances in $YbAu_{1.04}Ga_{0.96}$.

Atoms	d (Å)	Atoms	d (Å)	Atoms	d (Å)
Yb−1Au	3.043(1)	Au–2T	2.616(1)	T−2Au	2.616(1)
2Au	3.1144(8)	1T	2.629(2)	1Au	2.629(2)
2T	3.115(2)	1T	2.846(2)	1Au	2.846(2)
1T	3.150(2)	1Yb	3.043(1)	2Yb	3.115(2)
1T	3.180(2)	2Yb	3.1144(8)	1Yb	3.150(2)
2Au	3.1966(8)	2Yb	3.1966(8)	1Yb	3.180(2)
2T	3.275(2)	1Yb	3.351(1)	2Yb	3.275(2)
1Au	3.351(1)				
2Yb	3.626(1)				
2Yb	3.877(1)				

phase map. In an IPF map the local crystal direction normal to the surface is marked according to a colour-coded inverse pole figure.

2.5. Thermal analysis

Differential thermal analysis (DTA) and differential scanning calorimetry (DSC) were performed using an STA 409C NETZSCH device (Al_2O_3 crucibles, sample mass ~100 mg) under dynamic argon atmosphere in the temperature range of 30–1200 °C with heating rates of 2, 5 and 10 °C/min. The calibration was done using five melting standards (thermocouple type S).

2.6. Magnetization, electrical resistivity and XAS

The magnetization was measured in the temperature range 1.8–400 K in various applied magnetic fields up to $\mu_0 H=7$ T using a SQUID magnetometer (MPMS-XL7, Quantum Design).

The electrical resistivity of selected samples was measured between 4 K and 320 K by a conventional four-point method using direct current. Electrical contacts were made with silver-filled epoxy. The estimated inaccuracy of $\rho(T)$ of ±30% is due to the contact geometry and the small size of the investigated specimens.

The valence state of Yb was investigated by X-ray absorption spectroscopy at the Yb L_{III} edge. The spectra were recorded in transmission arrangement at the EXAFS II beamline E4 of the Hamburg synchrotron radiation laboratory (HASYLAB) at DESY. Wavelength selection was realized by means of a Si (111) double crystal monochromator which yields an energy resolution of approximately 2 eV (FWHM) at the Yb L_{III} threshold of 8944 eV. Experimental data were measured using Yb_2O_3 as an external reference. The spectra deconvolution and evaluation of the average valence of Yb atoms was made using the program XASWin [13].

3. Results and discussion

3.1. Crystal structure of $YbAu_{1.04}Ga_{0.96}$

The crystal structure of $YbAu_{1.04}Ga_{0.96}$ is of the TiNiSi type (space group *Pnma*, Fig. 1). Contrary to the literature data ([2], KHg_2 type, space group *Imma*) we found a practically complete Au/Ga ordering for this composition. The ordering of Au and Ga atoms is supported by a flattening of the Au-Ga framework, the body-centring translation of the lattice of the KHg_2-type subcell disappears, which leads to a *klassensgleiche* symmetry reduction of index 2 (*k*2) [14]. This is indicated by the presence of relatively strong primitive reflections in the powder as well as in the single-crystal diffraction data.

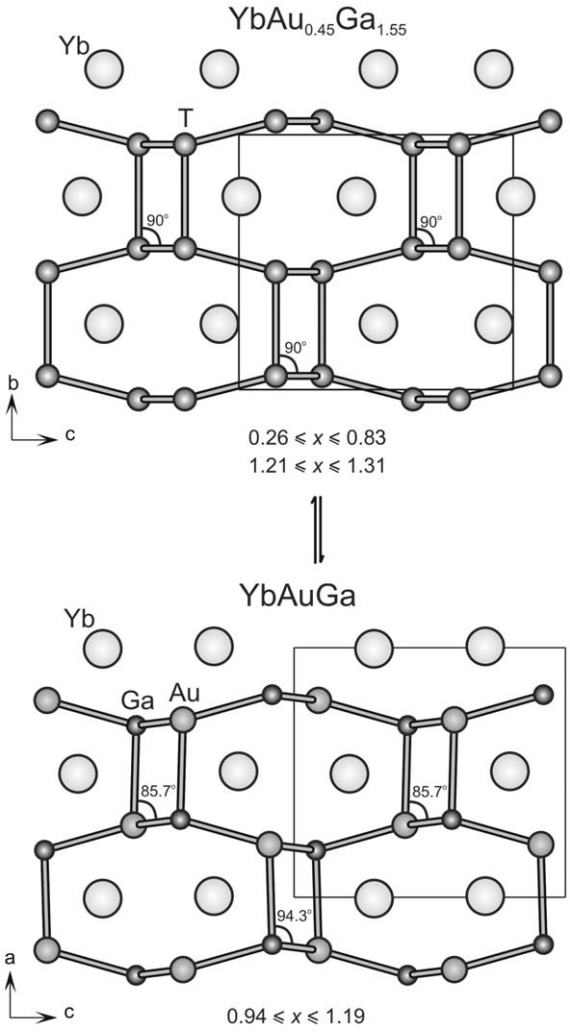

Fig. 1. Crystal structures of YbAuGa (TiNiSi type, space group *Pnma*) and $YbAu_{0.45}Ga_{1.55}$ (KHg_2 type, space group *Imma*).

Gold and gallium atoms in the crystal structure of $YbAu_{1.04}Ga_{0.96}$ alternate within condensed $[Au_3Ga_3]$ hexagons forming puckered nets perpendicular to [1 0 0]. The intralayer Au−Ga distances of 2.616(1) Å and 2.629(2) Å are close to the sum of Pauling's single bond radii of 2.581 Å (r(Au)=1.336 Å, r(Ga)=1.245 Å) [15]. Taking into account that the shortest interlayer Au−Ga distance of 2.846(2) Å is significantly longer we can state a

pronounced 2D character of the [AuGa] network in the structure of $YbAu_{1.04}Ga_{0.96}$. The coordination environments of Au as well as Ga atoms are formed by six Yb atoms in the form of strongly distorted trigonal prisms.

Ytterbium atoms in the crystal structure of $YbAu_{1.04}Ga_{0.96}$ are situated between two puckered $[Au_3Ga_3]$ rings, thus having in their coordination sphere 6 Au and 6 Ga atoms. The Yb–Au as well as Yb–Ga distances cover rather large intervals of 3.042(1)–3.351(1) Å and 3.114(2)–3.274(2) Å, respectively. In addition, each ytterbium atom has four nearest ytterbium neighbours at distances 3.626(1) Å (2×) and 3.877(1) Å (2×). The two shorter contacts correspond to Yb–Yb interaction along [1 0 0] and build infinite zigzag chains. The two longer interactions occur to the atoms situated in the (1 0 0) plane. The latter contacts are practically equal to the shortest distance in the *ccp* structure of elemental ytterbium [16].

3.2. Temperature-driven phase transition of YbAuGa

Differential scanning calorimetry (DSC) performed on the sample with the equiatomic composition YbAuGa clearly shows three endothermal effects at 629 °C, 774 °C and 990 °C (Fig. 2). Nevertheless, X-ray powder patterns obtained from samples annealed at 700 °C, 900 °C and 1100 °C, which were subsequently quenched, as well as those obtained after DSC experiment still contained diffraction reflections corresponding exclusively to YbAuGa phase with TiNiSi structure type. It should be also noted that with the increase of the heating rate the intensity of the DSC signal at ~630 °C decreases. It is remarkable that all body-centred reflections ($h+k+l=2n$) were sharp whereas all primitive reflections became fuzzy and have reduced intensities. This may be caused by the fast $KHg_2 \leftrightarrow$ TiNiSi transformation, which cannot be completely quenched. To investigate this problem in detail, *in-situ* high-temperature diffraction experiments using synchrotron radiation were performed.

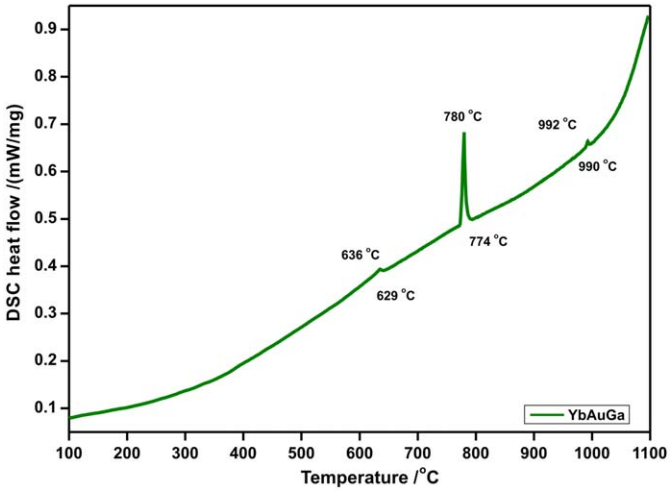

Fig. 2. (Colour online) DSC curve of YbAuGa sample. Heating rate 2 K/min. (The numbers below and above the curve correspond to the onset and peak temperatures, respectively.)

Selected synchrotron powder patterns are presented in Fig. 3. The dependence of the lattice parameters in YbAuGa (TiNiSi type, space group *Pnma* and KHg_2 type, in *Immb* setting) vs temperature as well as the DSC heating curve are shown in Fig. 4. With increasing temperature the reflections corresponding to the primitive lattice become fuzzy and disappear completely in the patterns measured above 650 °C. In the temperature region up to 500 °C the thermal expansion shows anisotropic character and for the lattice parameter *a* it is even negative. We assume that this behaviour is mainly connected with the flattening of the [AuGa] polyanion (see Fig. 1). In the temperature range of ~500–650 °C the thermal expansion becomes isotropic. The decrease of the intensities of the primitive reflections in this temperature interval is explained by a gradual destruction of the long-range order in the [AuGa] network. Finally, between the temperatures of 650 °C and 790 °C, only the atomic arrangement of the KHg_2 type exists. Starting from 790 °C the powder diffractograms contain lines of the additional unidentified phase. Thus, the two signals at 629 °C and 774 °C observed during DSC measurement were confirmed to be associated to the order-disorder transition (from TiNiSi to KHg_2 structure types) and (peritectic) decomposition of YbAuGa, respectively.

3.3. Homogeneity ranges

A series of samples $YbAu_xGa_{2-x}$ ($0.21 \le x \le 1.35$) was prepared with the aim to establish a possible homogeneity range of YbAuGa and explain an anomaly in the increase of the unit cell volume of $YbAu_{0.5}Ga_{1.5}$ phase (KHg_2 type) in comparison with those found for the equiatomic compound (see Introduction). All X-ray powder diffractograms collected from the samples with $0.94 \le x \le 1.19$,

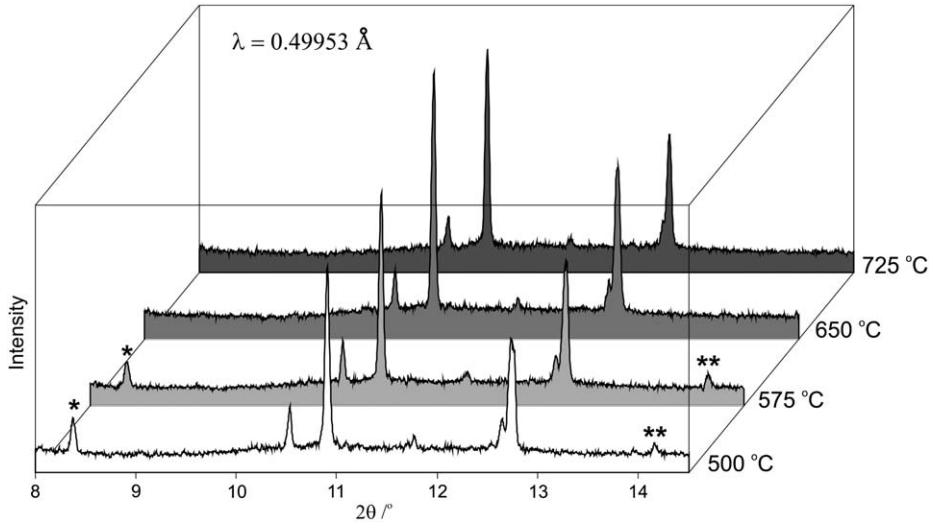

Fig. 3. Selected powder diffraction patterns of YbAuGa obtained at different temperatures using synchrotron radiation. The primitive reflections are marked by one (111 and 102) and two (311 and 302) asterisks at diagrams recorded at 500 °C and 575 °C.

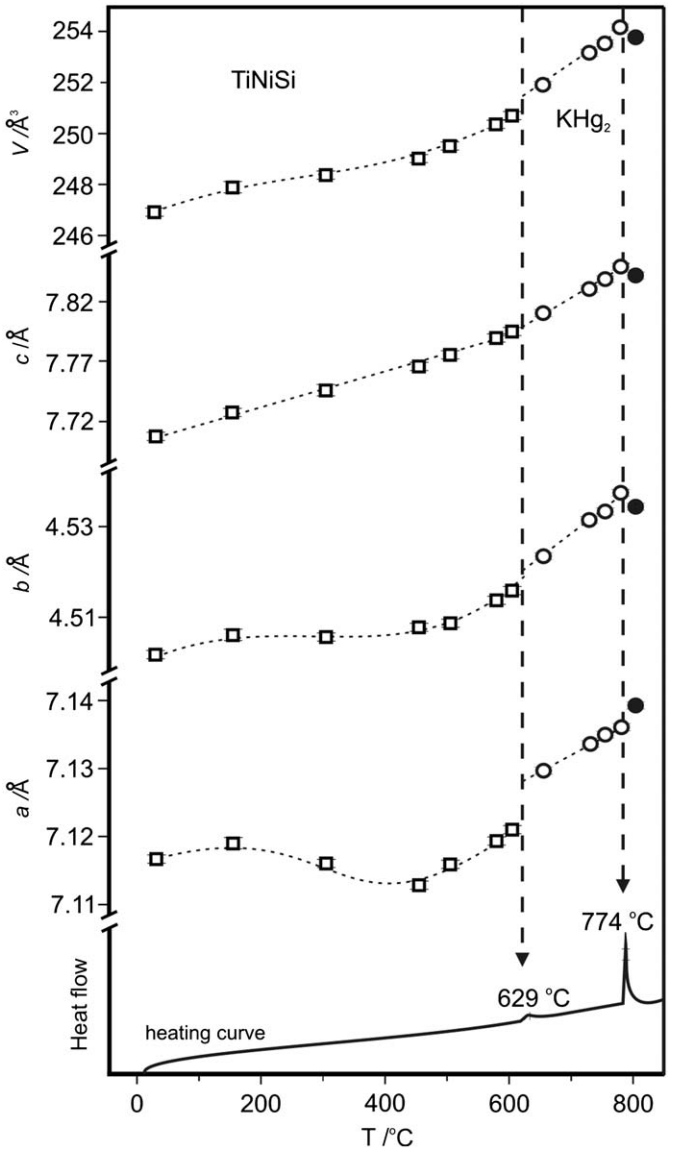

Fig. 4. Temperature dependence of the unit cell parameters of YbAuGa and DSC heating curve. For the temperature region of 650 – 790 °C the unit cell parameters for the crystal structure of KHg_2 type are given in the *Immb* setting.

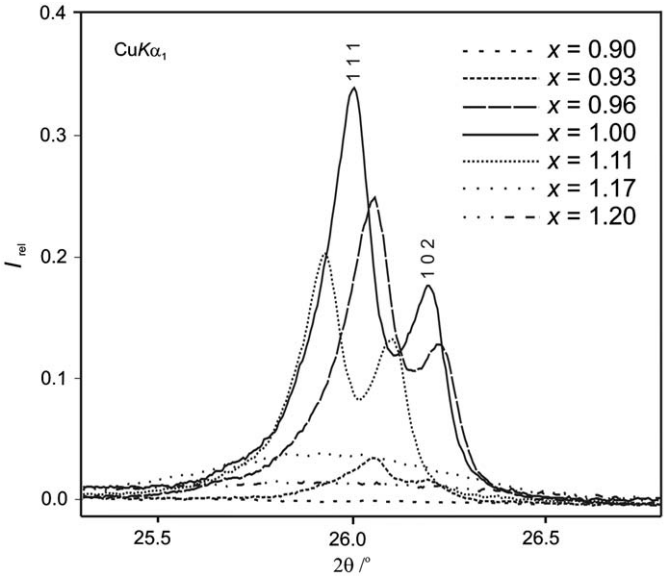

Fig. 5. Intensities and positions of the strongest reflections in the $YbAu_xGa_{2-x}$ compounds corresponding to the primitive lattice.

Table 4
Lattice parameters of $YbAu_xGa_{2-x}$ compounds[a].

x	a (Å)	b (Å)	c (Å)	V (Å^3)
0.21[b,c]	7.2466(8)	4.4836(6)	7.6738(9)	249.33(9)
0.24[b,c]	7.2478(6)	4.4831(4)	7.6757(5)	249.40(6)
0.27[c]	7.2446(6)	4.4830(4)	7.6739(5)	249.23(6)
0.45[c]	7.1911(8)	4.4794(5)	7.7189(6)	248.64(7)
0.54[c]	7.1713(8)	4.4804(4)	7.7295(7)	248.35(7)
0.72[c]	7.1499(4)	4.4857(2)	7.7283(2)	247.86(3)
0.84[b,c,d]	7.1396(8)	4.4904(4)	7.7204(5)	247.51(7)
0.90[b,c,d]	7.1366(8)	4.4894(4)	7.7141(7)	247.15(7)
0.93[b,c,d]	7.1305(4)	4.4918(4)	7.7129(3)	247.03(4)
0.96[d]	7.1188(3)	4.4994(3)	7.7101(4)	246.96(4)
1.00[d]	7.1167(3)	4.5019(3)	7.7083(3)	246.96(4)
1.02[d]	7.1153(3)	4.5047(3)	7.7100(4)	247.12(4)
1.08[d]	7.1157(3)	4.5106(3)	7.7246(3)	247.93(4)
1.11[d]	7.1188(5)	4.5155(2)	7.7350(4)	248.64(4)
1.17[d]	7.1209(5)	4.5237(6)	7.7544(4)	249.79(6)
1.20[b,c,d]	7.1218(5)	4.5276(3)	7.7649(4)	250.38(5)
1.28[c]	7.1180(4)	4.5414(2)	7.7925(3)	251.89(4)
1.35[b,c]	7.1192(5)	4.5399(5)	7.7878(4)	251.70(5)

[a] Lattice parameters of samples with KHg_2 type of structure are presented in this table in *Immb* setting.
[b] Two-phases sample (they were indexed assuming *Pnma* space group).
[c] KHg_2 type of crystal structure.
[d] TiNiSi type of crystal structure.

i.e., with a composition around to the equiatomic, can be described on the basis of the TiNiSi model. Nevertheless, the intensities of the primitive reflections decrease as the composition of the sample deviates from the equiatomic one (Fig. 5). This can be explained by a breaking of the long-range order due to partial replacement of Ga atoms by Au species in the [AuGa] network and *vice versa*. X-ray powder patterns obtained from $YbAu_xGa_{2-x}$ samples with $0.26 \le x \le 0.83$ and $1.21 \le x \le 1.31$ contain only reflections of the body-centred unit cell. The intensities can be described on the basis of the KHg_2-type model with statistical distribution of the Au and Ga atoms in the 8 *h* position. The refined lattice parameters for all synthesized samples are presented in Table 4 and in Fig. 6.

It is remarkable that, starting from the equiatomic composition, unit cell volume increases with decreasing as well as with increasing Au content. This finding agrees very well with the results obtained previously for YbAuGa [1,2] and $YbAu_{0.5}Ga_{1.5}$ [3]. To explain this behaviour X-ray absorption spectroscopy experiments were performed to establish the valence state of Yb.

Taking into account the close relationship between KHg_2 and TiNiSi types, and in our case, also close compositions of Yb-Au-Ga compounds crystallizing with these types, it was impossible to observe powder pattern reflections corresponding to both structure types simultaneously since all of them with $h+k+l=2n$ overlap. On the other hand clearly recognizable kinks in the plot for *a* and *b* at $x=0.93$ and for the lattice parameter *c* at $x=1.20$ (Fig. 6) are observed. Powder patterns of these samples reveal lower relative intensities of reflections with $(h+k+l=2n+1)$. So, they may be assumed to contain phases with TiNiSi as well as with KHg_2 types of crystal structure. Splitting of *h*00, 0*k*0, 0*l*0 or other reflections containing index 0 at high values of 2θ angle was also expected in these samples. Such splitting could be possibly due to a difference in the lattice parameters for phases with different Au content. Two reflections 0 4 0 and 0 2 6 have been analysed exemplarily: they show neither small intensities nor

splitting up to high Au-concentration (x=1.20). The full-width of half maximum (FWHM) of these reflections was studied in details for all samples using the WinCSD software [7]. The dependence of FWHM of the 0 4 0 reflection vs x is presented in Fig. 6: for most of the samples it is within the range 0.17°–0.21°. Significantly broader line shapes with FWHM(0 4 0) > 0.25° have been found for x=0.9, 0.93 and 1.20. The broad reflections could be successfully described as two peaks with FWHM which would correlate with the common dependence of FWHM *vs* 2θ. The same effect was observed for FWHM of the 0 2 6 reflection showing $0.17^\circ < \mathrm{FWHM}(0\,2\,6) < 0.20^\circ$ for single phase sample and broader lines with FWHM(0 2 6) > 0.23° for x=0.9, 0.93 and 1.20. The analysis of the powder diffraction patterns indicates that both orthorhombic phases with slightly different lattice parameters are present for compositions $YbAu_xGa_{2-x}$ with $x \approx 0.9$ and $x \approx 1.2$.

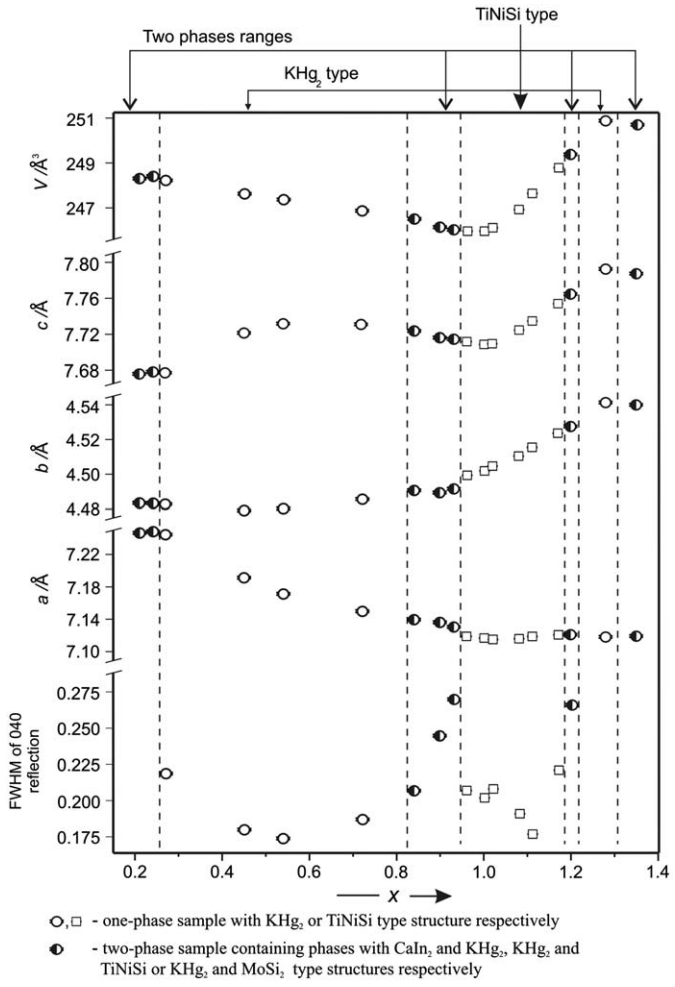

Fig. 6. Unit cell parameters of $YbAu_xGa_{2-x}$ and full-width at half maximum (FWHM) of the 0 4 0 reflection vs Au content x.

Investigations by electron backscattering diffraction (EBSD) confirmed the co-existence of both orthorhombic phases in the $YbAu_{0.9}Ga_{1.1}$ sample. The formation of less reflector bands and different intensities of selected bands leads to slightly different EBSD patterns for the phases with KHg_2 type and TiNiSi type of crystal structure (Fig. 7). Discrimination of both phases based on the consistence between calculated and measured bands and resulted in an almost homogenous phase distribution for both orthorhombic phases in the EBSD investigated area (Fig. 8a).

Optical bright-field images and material contrast images (BSE) of a much larger field than the EBSD investigated area of the $YbAu_{0.9}Ga_{1.1}$ microstructure showed minor amounts of well rounded particles. The matrix itself appears homogenous in BSE and in light-microscopic bright-field mode, however large portion of the matrix showed well defined contrast in polarized light. Particle size and distribution correspond to the phase map of the EBSD analyses which indicates that both contrasts originate from the co-existence of both orthorhombic phases. EDXS analyses confirmed the ratio of Yb:Au:Ga=1:0.9:1.1 for the matrix.

The results of the EBSD analyses support the interpretation of the broad reflections in the X-ray powder diffractograms by nearly coincident lines of both orthorhombic phases. The samples $YbAu_xGa_{2-x}$ with $0.26 \le x \le 0.83$ and $1.21 \le x \le 1.31$ contain only the phase with KHg_2 type of crystal structure. The phase with TiNiSi structure type has the intermediate composition range $0.94 \le x \le 1.19$. The large, μm-sized domains of both phases identified in the microstructure of $YbAu_{0.9}Ga_{1.1}$ sample confirm the presence of both phases at $0.83 < x < 0.94$. In analogy, it is reasonable to assume that near the composition $YbAu_{1.2}Ga_{0.8}$ both orthorhombic phases also co-exist.

3.4. X-ray absorption spectroscopy (XAS)

X-ray absorption spectra of the sample $YbAu_xGa_{2-x}$ near the Yb L_{III} edge (Fig. 9) contain two contributions corresponding to $4f^{14}$ (Yb^{+2}) and $4f^{13}$ (Yb^{+3}) ground states of Yb, i.e., indicate an intermediate valence state of ytterbium. The spectra obtained

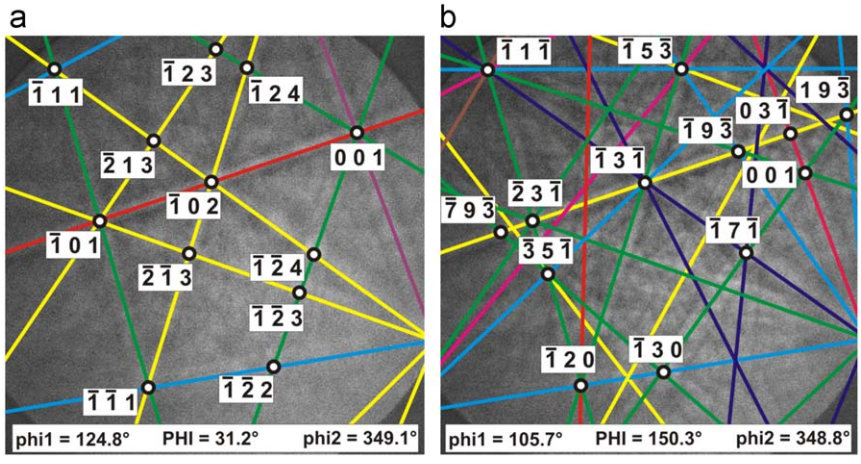

Fig. 7. (Colour online) EBSD patterns of KHg_2: (a) and TiNiSi and (b) phases. The KHg_2 phase has less reflector bands than *Pnma* and the (010) band (red) shows slightly stronger contrast than the corresponding (013) band for *Pnma*. (For interpretation of the references to colour in this figure legend, the reader is referred to the webversion of this article.)

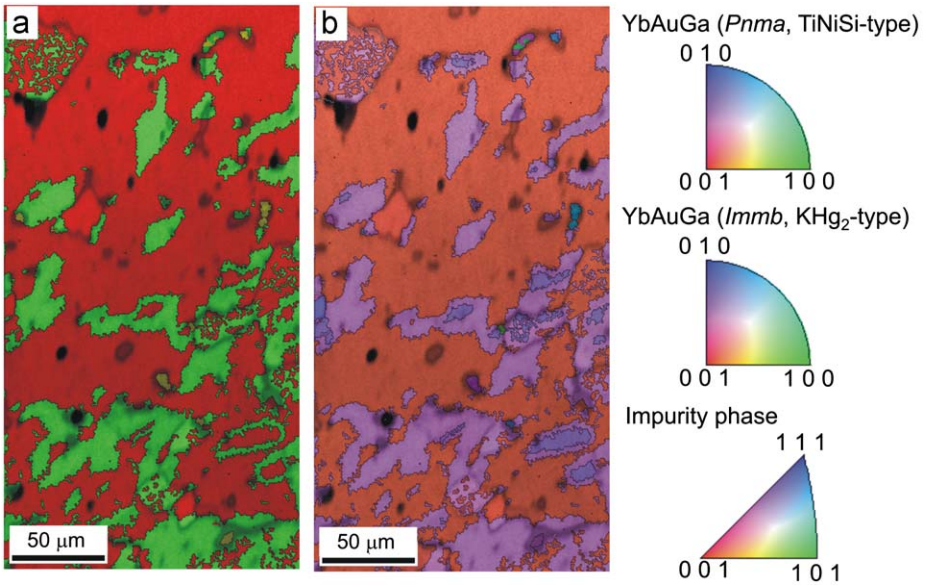

Fig. 8. (Colour online) (a) Overlay of a phase map and an IQ map of the sample $YbAu_{0.9}Ga_{1.1}$: TiNiSi phase (red), KHg_2 phase (green), third phase (yellow). (b) Overlay of an IPF map and an IQ map of the $YbAu_{0.9}Ga_{1.1}$ sample. The TiNiSi phase has two orientations (orange and blue), the KHg_2 phase in one orientation (pink). There are two distinct orientation relationships between TiNiSi and KHg_2 with a misorientation by 60° in respect to ⟨100⟩. (For interpretation of the references to colour in this figure legend, the reader is referred to the webversion of this article.)

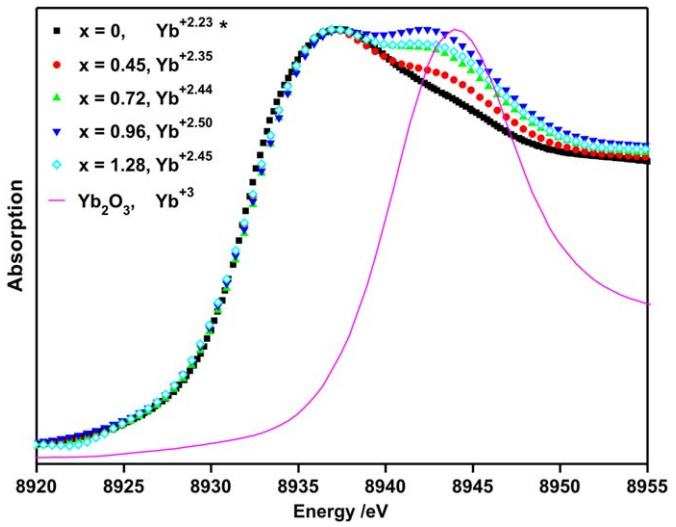

Fig. 9. (Colour online) Selected Yb L_{III} XAS for $YbAu_xGa_{2-x}$ (*—data taken from [17]).

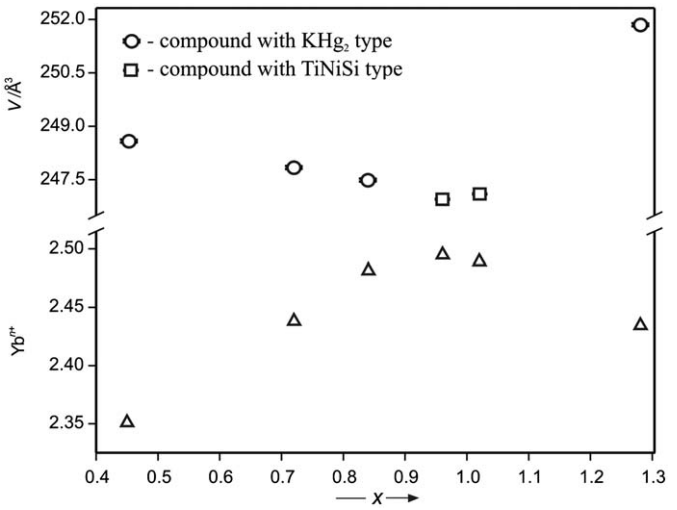

Fig. 10. Unit cell volumes of $YbAu_xGa_{2-x}$ and corresponding valence of Yb vs Au content x.

from the samples around the equiatomic composition contain practically equal contributions of both white lines (WL) reflecting nearly equal fractions of Yb in $4f^{14}$ (Yb^{+2}) and $4f^{13}$ (Yb^{+3}) configuration corresponding to an average valence of +2.5. The intensity of the high-energy line decreases with the deviation of the Au content from the 1:1:1 composition designating a reduced fraction of Yb in the $4f^{13}$ state. The average valence of Yb drops to +2.35 and +2.45 for $YbAu_{0.45}Ga_{1.55}$ and $YbAu_{1.28}Ga_{0.72}$, respectively. The decreasing valence of Yb is reflected in an increase of the unit cell volume of the samples with the composition deviating from the equiatomic one (Fig. 10). The slope of the $V(x)$ plot for $x<1$ is somewhat lower than for $x>1$ due to the complementary decrease of the unit cell volumes due to the replacement of part of Au atoms by smaller Ga species.

Study of the magnetic susceptibility suggests the Yb atoms to be in +2 oxidation state in the $YbGa_2$ ($x=0$) compound ($CaIn_2$ type of crystal structure), which is in full agreement with Zintl-Klemm concept $Yb^{+2}(Ga^{-})_2$ model [17]. Starting with $5d^{10}6s^1$ electron configuration for Au atoms and $4s^24p^1$ for Ga atoms and taking into account, that they are four-bounded in the structure with KHg_2 type we assume them to be -3 and -1 respectively. Thus, our compounds may be written as $Yb^k[Au^{-3}]_x[Ga^{-1}]_{2-x}$, which completely misses the experimental facts ($x=1$ at $k=4$). Taking experimental $k=2.5$ and $(4b)Ga^{1-}$ we get $(4b)Au^{1.5-}$ for four-bonded gold atoms coordinated exclusively by gallium. Assuming that the disorder will result in formation of Au-Au bonds, the formal charge on gold should be reduced, leading to a reduction of the effective valence of Yb.

3.5. Magnetic susceptibility of $YbAu_xGa_{2-x}$

The magnetic susceptibility $\chi=M/H$ ($\mu_0H=1$ T) of samples from the series is given in Fig. 11. $\chi(T)$ is small indicating a

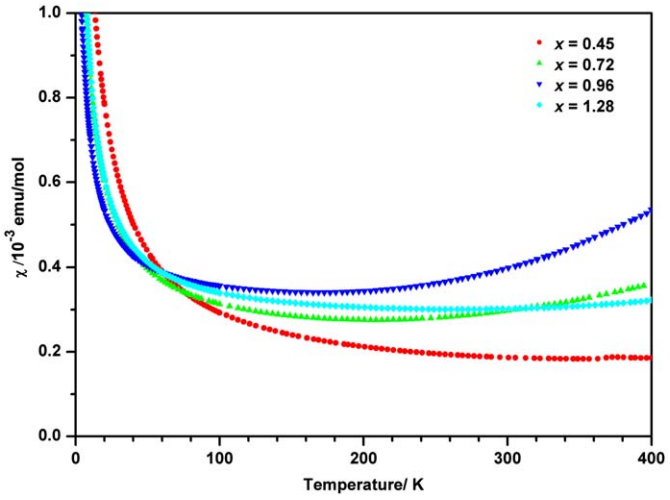

Fig. 11. (Colour online) Temperature dependence of the magnetic susceptibility $\chi(T)$ of $YbAu_xGa_{2-x}$ for various x in $\mu_0H=1$ T.

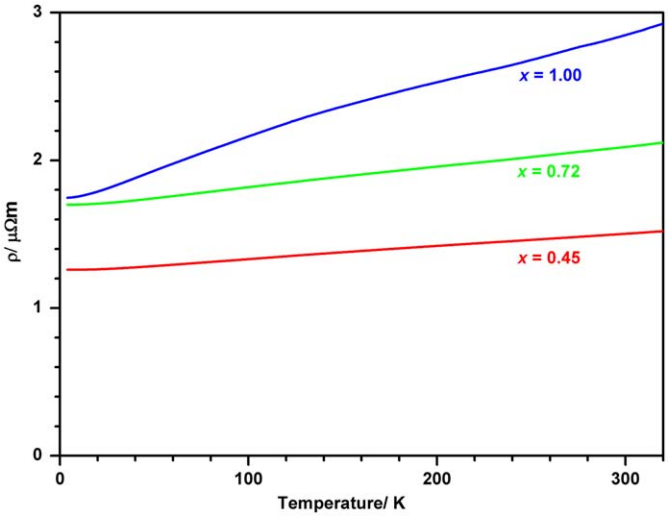

Fig. 12. (Colour online) Electrical resistivity $\rho(T)$ of selected $YbAu_xGa_{2-x}$ samples.

non-magnetic $4f^{14}$ ground state. The temperature-independent term χ_0 of the susceptibility is enhanced (x=0.45, 0.13×10^{-3}; x=0.72, 0.18×10^{-3}; x=0.96, 0.25×10^{-3}; x=1.28, 0.25×10^{-3} emu/mol). The upturn of $\chi(T)$ towards the lowest temperatures is most likely due to minor paramagnetic impurities which follow the Curie law with $\mu_{eff}\approx0.2\,\mu_B$, corresponding to $\approx0.2\,\%$ Yb^{3+} impurities (e.g. as Yb_2O_3). Except for one sample (x=0.45) a more or less strong upturn of $\chi(T)$ is observed for the highest temperatures. The amplitude of this upturn increases with increasing Au-content x and decreases suddenly beyond $x\approx1$. This is consistent with the variation of both the valence obtained from XAS and the lattice cell volume with x (Fig. 11) and indicates thermal fluctuations towards the $4f^{13}$ state of Yb [18] with a magnetic $^2F_{7/2}$ crystal-field ground multiplet.

3.6. Electrical resistivity

The electrical resistivity $\rho(T)$ of the samples with x=0.45, x=0.72 and x=1 (Fig. 12) confirms the metallic character of the investigated compositions of $YbAu_xGa_{2-x}$. The residual resistivity of the compounds is high ($\rho_0\approx1.0$–$1.7\,\mu\Omega$ m) while the temperature-dependent contribution ($\rho(300\,K)-\rho_0$) is much smaller (0.18–0.40 μΩ m). This is partially due to the brittleness of the investigated coarse-grained polycrystalline pieces. Without suitable single crystals of this substitution series no reliable conclusions can be drawn on the possible influence of structural disorder on the residual resistivity.

4. Conclusions

The YbAuGa compound has been shown to crystallize with the TiNiSi type of structure at 600 °C. At this temperature YbAuGa possess a homogeneity range $YbAu_xGa_{2-x}$, where $0.94\le x\le1.19$. A DSC study and an *in-situ* high-temperature diffraction experiment showed that the equiatomic compound undergoes a structural phase transition at 629 °C from ordered TiNiSi to disordered KHg_2 structure type. $YbAu_xGa_{2-x}$ in the gallium-($0.26\le x\le0.83$) and gold-rich ($1.21\le x\le1.31$) regions crystallizes with the KHg_2 type of crystal structure with mixed Au/Ga occupation 8*h* crystallographic position (space group *Imma*). Since X-ray powder patterns of the $YbAu_xGa_{2-x}$ compounds crystallizing with KHg_2 and TiNiSi structure types differ just by the presence of some primitive reflections, analysis of FWHM and EBSD were successfully used to find two phase regions. The Yb L_{III} X-ray absorption spectroscopy and magnetic susceptibility studies indicate an intermediate valence of Yb in the $YbAu_xGa_{2-x}$ compounds which decreases with the deviation from the equiatomic composition. The compounds are metallic conductors with large residual resistivities.

Acknowledgements

The authors thank P. Scheppan and M. Eckert for the preparation of metallographic microstructure as well as for EDXS measurements, S. Müller and S. Hoffmann for differential thermal analysis experiments, E. Welter, D. Zajats and D. Trots from HASYLAB for helpful assistance during XAS measurements and in-situ high-temperature diffraction experiment. R. Gumeniuk is grateful to the Deutscher Akademischer Austauschdienst (DAAD) for a research fellowship.

Appendix A. Supplementary material

Supplementary data associated with this article can be found in the online version at doi:10.1016/j.jssc.2009.09.015.

Supplementary data for this paper are available from the FIZ, D-76344 Eggenstein-Leopoldshafen, Germany, e-mail crysdata@FIZ-karlsruhe.de, by quoting the depository number 420780.

References

[1] L.C. Gupta, S.K. Malik, in: Proceedings of the 5th International Conference on Valence Fluctuations, Bangalore, 1987, p. 463.
[2] D. Rossi, R. Ferro, J. Alloys Compd. 317–318 (2001) 521.
[3] D. Rossi, R. Ferro, Intermetallics 8 (2000) 877.
[4] [a] F. Merlo, M. Pani, M.L. Fornasini, J. Alloys Compd. 232 (1996) 289; [b] M.D. Bojin, R. Hoffmann, Helv. Chim. Acta 86 (2003) 1653.
[5] J. Emsley, The Elements, Oxford University Press, Oxford, 1998.
[6] R. Gumeniuk, Yu. Prots, M. Schmidt, W. Schnelle, Yu. Kuz'ma, Yu. Grin, in: Book of Abstracts of 15th Conference on Solid Compounds of Transition Elements, Kraków, 2006, p. 10.
[7] L.G. Akselrud, P.Yu. Zavalij, Yu.N. Grin, V.K. Pecharsky, B. Baumgartner, E. Wölfel, Mater. Sci. Forum 333–335 (1993) 133.

[8] M. Knapp, V. Joco, C. Baehtz, H.H. Brecht, A. Ehrenberg, H. Seggern, H. Fuess, Nucl. Instrum. Methods A 521 (2004) 565.
[9] D. Kußmann, R.-D. Hoffmann, R. Pöttgen, Z. Anorg. Allg. Chem. 624 (1998) 1727.
[10] [a] X-RED, Version 1.10, STOE Data Reduction Program, STOE & Cie GmbH, Darmstadt, 1998.;
[b] XSHAPE, Version 1.06, Crystal Optimisation for Numerical Absorption Correction, STOE & Cie GmbH, Darmstadt, 1999.
[11] C.B. Shoemaker, D.P. Shoemaker, Acta Crystallogr. 18 (1965) 900.
[12] D.T. Adroja, B.D. Rainford, S.K. Malik, M. Gailloux, K.A. Gschneider, Phys. Rev. B 50 (1994) 248.
[13] L.G. Akselrud, Yu. Grin, XASWin Program, Max-Planck-Institut für Chemische Physik fester Stoffe, Dresden, 2004.
[14] R.-D. Hoffmann, R. Pöttgen, Z. Kristallogr. 216 (2001) 127.
[15] L. Pauling, The Chemical Bond, Cornell University Press, Ithaca, NY, 1967.
[16] J. Donohue, The Structures of the Elements, Wiley, New York, 1974.
[17] U. Schwarz, R. Giedigkeit, R. Niewa, M. Schmidt, W. Schnelle, R. Cardoso, M. Hanfland, Z. Hu, K. Klementiev, Yu. Grin, Z. Anorg. Allg. Chem. 627 (2001) 2249.
[18] U. Schwarz, M. Schmidt, R. Gumeniuk, W. Schnelle, M. Hanfland, K. Klementiev, Yu. Grin, Z. Anorg. Allg. Chem. 630 (2004) 122.